ACADEMIC PRESS

Available online at www.sciencedirect.com

SCIENCE DIRECT®

Journal of Sound and Vibration 261 (2003) 791–804

JOURNAL OF SOUND AND VIBRATION

www.elsevier.com/locate/jsvi

Phase shift and attenuation characteristics of acoustic waves in a flowing gas confined by cylindrical walls

M. Willatzen*

Mads Clausen Institute for Product Innovation, University of Southern Denmark, Grundtvigs Alle 150, DK-6400 Sønderborg, Denmark

Received 23 May 2001; accepted 1 May 2002

Abstract

Wave propagation in flowing ideal gases confined by cylindrical waveguides is described in the low-frequency range using an iterative Frobenius series expansion method. The primary concern is to present a mathematical model enabling any radial-dependent flow profile to be analyzed. In contrast to previous analytical results, the present model is applicable in the general case where cubic and higher order terms in the axial acoustic velocity become important and to examine the influence of a non-vanishing radial velocity term. As a numerical test case, it is found that a gas flow velocity $w(r)$—for simplifying reasons assumed to be a linear combination of a flat flow profile and a parabolic flow profile corresponding to a mean flow equal to $\bar{w}$—is well approximated by a flat flow profile of the same mean flow value $\bar{w}$ at low shear wavenumbers and at higher shear wavenumbers (calculations were done for shear wavenumbers up to 8). In actual fact, the error introduced by making this mean flow approximation is smaller than the error introduced by neglecting the radial velocity term.

1. Introduction

The classical problem of sound propagation in gases contained in a cylindrical pipe has been extensively studied for the case of a quiet medium [1–5]. During the past two decades, many important results have been obtained for the propagation of acoustic waves in flowing gases including effects due to temperature gradients, heat conduction/convection, and viscosity [6–14].

Particular interest has been paid to wave propagation in catalytic converters being a standard component in present-day automobile exhaust systems [9–11]. Peat considered analytically the

*Tel.: +45-65-50-16-82; fax: +45-65-50-16-60.
E-mail address: willatzen@mci.sdu.dk (M. Willatzen).

0022-460X/02/$ - see front matter
PII: S0022-460X(02)00990-2

influence of a parabolic flow profile corresponding to laminar flow in capillary tubes of cylindrical cross-section by use of a variational principle [9]. In the case of wave propagation in non-isentropic flowing gases, it was assumed in Ref. [9] that radial velocity terms could be neglected and that the axial acoustic velocity was well represented by a quadratic expansion in the radial co-ordinate. A comparison between the model in Ref. [9] and exact results at zero flow [4] reveals that the approximation made in Ref. [9] leads to deviations at high shear wavenumbers (especially in terms of attenuation). Recent results by Peat and Kirby [13], however, include effects due to radial velocity terms as well as background temperature gradients but this work describes parabolic flow velocities only and is "purely" numerical. Dokumaci [11] presented a quasi-analytical solution to the problem of acoustic wave propagation in a flowing gas where the flow velocity is constant, i.e., independent of the radial co-ordinate.

In the present work, an iterative model based on the Frobenius power series expansion method is employed to examine wave propagation in a flowing gas including effects due to heat conduction/convection as well as viscosity. The steady state gas flow velocity can be any function of the radial co-ordinate. Results are finally given for the case where the steady state flow velocity is a linear combination of a constant flow profile (fully developed turbulent flow) and a parabolic flow profile (laminar flow).

2. Theory

Acoustic wave propagation in a flowing gas confined by cylindrical walls is governed by the continuity equation, the Navier–Stokes equations, the energy equation, and the equation of state. In the following, it will be assumed that the gas flow velocity $w(r)$ can be represented as an infinite power series in the radial co-ordinate r:

$$w(r) = \sum_{\lambda=0}^{\infty} w_\lambda r^\lambda, \tag{1}$$

where w_λ is the λth expansion coefficient of $w(r)$ with respect to r. In the case where acoustic wavelengths are much larger than the cylinder radius, it is reasonable to apply the conventional boundary layer approximations that the axial velocity u^* is much larger than the radial velocity v^* and that changes in the radial direction are much larger than those in the axial direction (z direction) [9,10]

$$u^* \gg v^*, \quad \frac{\partial}{\partial r} \gg \frac{\partial}{\partial z}. \tag{2}$$

Under axisymmetric excitation conditions, azimuthal dependencies vanish identically by symmetry

$$\frac{\partial}{\partial \theta} = 0 \tag{3}$$

and the basic dynamic equations governing acoustics in flowing (ideal) gases simplify to

$$p^* = \rho^* R_0 T^*, \tag{4}$$

$$\frac{\partial \rho^*}{\partial t} + u^* \frac{\partial \rho^*}{\partial z} + v^* \frac{\partial \rho^*}{\partial r} + \rho^* \left(\frac{\partial v^*}{\partial r} + \frac{v^*}{r} + \frac{\partial u^*}{\partial z} \right) = 0, \tag{5}$$

$$\rho^* \left(\frac{\partial u^*}{\partial t} + v^* \frac{\partial u^*}{\partial r} + u^* \frac{\partial u^*}{\partial z} \right) = -\frac{\partial p^*}{\partial z} + \mu \left(\frac{\partial^2 u^*}{\partial r^2} + \frac{1}{r} \frac{\partial u^*}{\partial r} \right), \tag{6}$$

$$\frac{\partial p^*}{\partial r} = 0, \tag{7}$$

$$\rho^* c_p \left(\frac{\partial T^*}{\partial t} + v^* \frac{\partial T^*}{\partial r} + u^* \frac{\partial T^*}{\partial z} \right) = \frac{\partial p^*}{\partial t} + K \left(\frac{\partial^2 T^*}{\partial r^2} + \frac{1}{r} \frac{\partial T^*}{\partial r} \right) + u^* \frac{\partial p^*}{\partial z} + \mu \left(\frac{\partial u^*}{\partial r} \right)^2. \tag{8}$$

Here, ρ^*, p^*, and T^* are the fluid density, pressure, and temperature, respectively, R_0 is the gas constant, μ is the first viscosity (the second viscosity coefficient is neglected in the present work for simplifying reasons), K is the thermal conductivity, and c_p is the heat capacity at constant pressure. Next, under monofrequency excitation conditions ($\exp(\mathrm{i}\omega t)$ time dependence), dependent variables are separated into steady state terms and acoustic terms as follows:

$$\rho^* = \bar{\rho}[1 + \alpha\rho(\eta)\exp(\Gamma\zeta + \mathrm{i}\omega t)], \tag{9}$$

$$u^* = \bar{a}[M_0(\eta) + \alpha u(\eta)\exp(\Gamma\zeta + \mathrm{i}\omega t)], \tag{10}$$

$$v^* = \bar{a}\alpha v(\eta)\exp(\Gamma\zeta + \mathrm{i}\omega t), \tag{11}$$

$$p^* = \frac{\bar{\rho}\bar{a}^2}{\gamma}[P_0(\zeta) + \alpha p(\eta)\exp(\Gamma\zeta + \mathrm{i}\omega t)], \tag{12}$$

$$T^* = \frac{\bar{a}^2}{\gamma R_0}[1 + \alpha T(\eta)\exp(\Gamma\zeta + \mathrm{i}\omega t)], \tag{13}$$

where α is a perturbative dimensionless parameter. In addition, the following dimensionless co-ordinates have been introduced in Eqs. (9)–(13):

$$\zeta = \frac{\omega z}{\bar{a}}, \tag{14}$$

$$\eta = \frac{r}{R} \tag{15}$$

and

$$M_0(\eta) = \frac{w(\eta)}{\bar{a}} = \frac{1}{\bar{a}} \sum_{\lambda=0}^{\infty} w_\lambda (\eta R)^\lambda. \tag{16}$$

In Eqs. (9)–(13), $\alpha \ll 1$ as acoustic fluctuations are considered small, R is the cylinder radius, $\bar{\rho}$ and $\bar{a}$ denote the steady state mass density and sound speed, respectively, $P_0(\zeta)$ is the steady state pressure being a function of the axial co-ordinate only (refer to Eq. (7)), and $\gamma = c_p/c_v$ is the ratio of specific heats. It is convenient to introduce explicit notations for the real and imaginary parts of the complex propagation constant Γ in the following:

$$\Gamma = \Gamma' + \mathrm{i}\Gamma'', \tag{17}$$

where Γ' represents attenuation of acoustic waves per unit distance and Γ'' is the phase shift over the same distance.

Linearized acoustic equations follow from equating terms to first order in α obtained by inserting Eqs. (9)–(13) into the governing equations (4)–(8), and read

$$k[\mathrm{i}\rho + \Gamma u + M_0(\eta)\rho] + \frac{\mathrm{d}v}{\mathrm{d}\eta} + \frac{v}{\eta} = 0, \tag{18}$$

$$\mathrm{i}u + M_0(\eta)\Gamma u(\eta) + \frac{\mathrm{d}M_0(\eta)}{\mathrm{d}\eta}\frac{v(\eta)}{k} = -\frac{\Gamma}{\gamma}p + \frac{1}{s^2}\left[\frac{\mathrm{d}^2u}{\mathrm{d}\eta^2} + \frac{1}{\eta}\frac{\mathrm{d}u}{\mathrm{d}\eta}\right], \tag{19}$$

$$\begin{aligned}\mathrm{i}T + M_0(\eta)\Gamma T = {} & \frac{1}{\sigma^2 s^2}\left[\frac{\mathrm{d}^2T}{\mathrm{d}\eta^2} + \frac{1}{\eta}\frac{\mathrm{d}T}{\mathrm{d}\eta}\right] + \frac{\gamma-1}{\gamma}[\mathrm{i} + M_0(\eta)\Gamma]p \\ & + \frac{\gamma-1}{s^2}\left[\frac{u(\eta)}{\eta}\frac{\mathrm{d}}{\mathrm{d}\eta}\left(\eta\frac{\mathrm{d}M_0(\eta)}{\mathrm{d}\eta}\right) + 2\frac{\mathrm{d}M_0(\eta)}{\mathrm{d}\eta}\frac{\mathrm{d}u(\eta)}{\mathrm{d}\eta}\right],\end{aligned} \tag{20}$$

$$p = \rho + T = \mathit{constant}, \tag{21}$$

where s is the so-called shear wavenumber given by

$$s = R\sqrt{\bar{\rho}\omega/\mu} \tag{22}$$

and

$$\sigma = \sqrt{Pr} = \sqrt{\mu c_p/K} \tag{23}$$

is the square-root of the Prandtl number Pr. Here, it should be mentioned that (following Ref. [9]), Eqs. (5) and (7) are satisfied identically to zeroth order in α, while Eq. (6) requires flow to fulfill: $M_0(\eta) = 2\bar{M}(1-\eta^2)$, i.e., flow is parabolic with mean flow $\bar{M}$. However, the state and energy equations (Eqs. (4) and (8)) are not satisfied by this steady parabolic flow solution, but this slight imbalance is neglected here. Furthermore, it will be assumed that the cylinder walls are rigid and characterized by a high thermal conductivity such that the boundary conditions

$$u = v = T = 0, \tag{24}$$

apply when $\eta = 1$. Eqs. (18)–(21) combined with the boundary condition Eq. (24) can be solved by use of the Frobenius series expansion method [15,16]. This procedure is described in the next section.

3. The Frobenius method applied to gas flow acoustics

In this section, an iterative procedure for solving Eqs. (18)–(21) and Eq. (24) is described using the Frobenius series expansion method. Let us start out by rewriting Eq. (19) as [15,16]

$$\frac{\mathrm{d}^2u^{i+1}}{\mathrm{d}\eta^2} + \frac{1}{\eta}\frac{\mathrm{d}u^{i+1}}{\mathrm{d}\eta} - \mathrm{i}s^2u^{i+1} = f^i(\eta), \tag{25}$$

where

$$f^i(\eta) = s^2\left(\frac{v^i(\eta)}{k}\frac{\mathrm{d}M_0(\eta)}{\mathrm{d}\eta} + \frac{\Gamma^i}{\gamma}p + M_0(\eta)u^i(\eta)\Gamma^i\right) = \sum_{\lambda=0}^{\infty} f_\lambda^i \eta^\lambda. \tag{26}$$

Here, u^i and u^{i+1} denote u values obtained at iteration steps i and $i+1$, respectively. Similar notation is used for v, T, ρ, and Γ. Recall that expressions for u^i, v^i, T^i, and ρ^i are known at iteration step i before determining updated values at iteration step $i+1$. The coefficients f_λ^i appearing in Eq. (26) are determined by performing an infinite power series expansion of $f^i(\eta)$ (this expansion is possible since $f^i(\eta)$ is known when u^i, v^i, T^i, and ρ^i are known. Furthermore, it is assumed that series expansions of u^i, v^i, T^i, and ρ^i are rendered possible at iteration step i).

Next, looking for u^{i+1} solutions on the form

$$u^{i+1}(\eta) = \sum_{\lambda=0}^{\infty} u_\lambda^{i+1}\eta^\lambda \tag{27}$$

one finds by insertion into Eq. (25) and employing the identity theorem for infinite power series that the recurrence relation

$$u_{\lambda+2}^{i+1} = \frac{f_\lambda^i + u_\lambda^{i+1}}{(\lambda+2)^2}, \quad \lambda = 0, 1, 2, 3, \ldots \tag{28}$$

must be fulfilled. Firstly, we are interested in finding a solution to Eq. (25). Let us consider the particular solution $u^{p,i+1}(\eta)$ for which the two first coefficients in Eq. (27) vanish, i.e., $u_0^{p,i+1} = u_1^{p,i+1} = 0$. Remaining coefficients: $u_\lambda^{p,i+1}$, $\lambda \geqslant 2$ are now completely determined from Eqs. (28) and (26), and so $u^{p,i+1}(\eta)$ is specified. The general solution $u^{i+1}(\eta)$ to Eq. (25) can be written as a sum of the general solution to the homogeneous differential equation:

$$\frac{\mathrm{d}^2u^{h,i+1}}{\mathrm{d}\eta^2} + \frac{1}{\eta}\frac{\mathrm{d}u^{h,i+1}}{\mathrm{d}\eta} - \mathrm{i}s^2u^{h,i+1} = 0 \tag{29}$$

and the particular solution $u^{p,i+1}(\eta)$ found above. The general solution $u^{h,i+1}(\eta)$ to Eq. (29) amenable with the condition: $\lim_{\eta\to 0}|u^{h,i+1}(\eta)| < \infty$ becomes

$$u^{h,i+1}(\eta) = A\mathrm{J}_0\left(\frac{s}{\sqrt{\mathrm{i}}}\eta\right) \tag{30}$$

and A is a constant uniquely determined by the boundary condition

$$u^{i+1}|_{\eta=1} = (u^{h,i+1} + u^{p,i+1})|_{\eta=1} = 0. \tag{31}$$

Imposing the latter condition immediately gives the exact solution to Eq. (25) at iteration step $i+1$:

$$u^{i+1}(\eta) = \sum_{\lambda=0}^{\infty} u_\lambda^{p,i+1}\eta^\lambda - \frac{\sum_{\lambda=0}^{\infty} u_\lambda^{p,i+1}}{\mathrm{J}_0(s/\sqrt{\mathrm{i}})}\mathrm{J}_0\left(\frac{s}{\sqrt{\mathrm{i}}}\eta\right). \tag{32}$$

Consider next the energy equation: Eq. (8), and rewrite it as

$$\frac{\mathrm{d}^2T^{i+1}}{\mathrm{d}\eta^2} + \frac{1}{\eta}\frac{\mathrm{d}T^{i+1}}{\mathrm{d}\eta} - \mathrm{i}\sigma^2s^2T^{i+1} = g^i(\eta) \tag{33}$$

in a similar iterative scheme as for u where now

$$g^i(\eta) = \sigma^2 s^2 \left[M_0(\eta)\Gamma^i T^i(\eta) - \frac{\gamma-1}{\gamma}[\mathrm{i} + M_0(\eta)\Gamma^i]p + \frac{\gamma-1}{s^2}\left[\frac{u^i(\eta)}{\eta}\frac{\mathrm{d}}{\mathrm{d}\eta}\left(\eta\frac{\mathrm{d}M_0(\eta)}{\mathrm{d}\eta}\right) + 2\frac{\mathrm{d}M_0(\eta)}{\mathrm{d}\eta}\frac{\mathrm{d}u^i(\eta)}{\mathrm{d}\eta}\right]\right] = \sum_{\lambda=0}^{\infty} g_\lambda^i \eta^\lambda. \tag{34}$$

Again, coefficients g_λ^i are easily determined from known series expansions of u^i, v^i, T^i, and ρ^i at iteration step i. The solution to Eq. (34) at iteration step $i+1$, satisfying the boundary condition: $T^{i+1}(\eta) = 0$ at $\eta = 1$, while being finite at the cylinder axis ($\lim_{\eta\to 0}|T^{i+1}(\eta)| < \infty$) is determined by carrying out an analogue procedure as in the case of the axial acoustic velocity $u(\eta)$. Eventually, it is found that

$$T^{i+1}(\eta) = \sum_{\lambda=0}^{\infty} T_\lambda^{p,i+1}\eta^\lambda - \frac{\sum_{\lambda=0}^{\infty} T_\lambda^{p,i+1}}{\mathrm{J}_0(\sigma s/\sqrt{\mathrm{i}})}\mathrm{J}_0\left(\frac{\sigma s}{\sqrt{\mathrm{i}}}\eta\right), \tag{35}$$

where

$$T_0^{p,i+1} = T_1^{p,i+1} = 0,$$
$$T_{\lambda+2}^{p,i+1} = \frac{g_\lambda^i + T_\lambda^{p,i+1}}{(\lambda+2)^2}, \quad \lambda = 0, 1, 2, 3, \ldots\ . \tag{36}$$

Having determined $T^{i+1}(\eta)$, density fluctuations $\rho^{i+1}(\eta)$ can be easily expressed as

$$\rho^{i+1}(\eta) = p - T^{i+1}(\eta) = p - \sum_{\lambda=0}^{\infty} T_\lambda^{p,i+1}\eta^\lambda + \frac{\sum_{\lambda=0}^{\infty} T_\lambda^{p,i+1}}{\mathrm{J}_0(\sigma s/\sqrt{\mathrm{i}})}\mathrm{J}_0\left(\frac{\sigma s}{\sqrt{\mathrm{i}}}\eta\right) = \sum_{\lambda=0}^{\infty}\rho_\lambda^{i+1}\eta^\lambda. \tag{37}$$

As a last step in closing the iteration loop, the continuity equation will be next employed. Eq. (18) can be rewritten as

$$\eta k\mathrm{i}\rho^{i+1}(\eta) + \eta k\Gamma^{i+1}u^{i+1}(\eta) + h^i(\eta) = -\frac{\mathrm{d}}{\mathrm{d}\eta}(\eta v^{i+1}(\eta)), \tag{38}$$

where

$$h^i(\eta) = M_0(\eta)k\Gamma^i\rho^i(\eta)\eta = \sum_{\lambda=0}^{\infty} h_\lambda^i\eta^\lambda. \tag{39}$$

Integration of Eq. (38) from $\eta = 0$ to 1 yields an expression for the updated Γ^{i+1}:

$$\Gamma^{i+1} = -\frac{1}{k}\frac{\sum_{\lambda=0}^{\infty} h_\lambda^i/(\lambda+1)}{\sum_{\lambda=0}^{\infty} u_\lambda^{i+1}/(\lambda+2)} - \mathrm{i}\frac{\sum_{\lambda=0}^{\infty}\rho_\lambda^{i+1}/(\lambda+2)}{\sum_{\lambda=0}^{\infty} u_\lambda^{i+1}/(\lambda+2)}. \tag{40}$$

As a corollary, integration of Eq. (38) from $\eta = 0$ to η allows $v^{i+1}(\eta)$ to be derived:

$$v^{i+1}(\eta) = -k\mathrm{i}\sum_{\lambda=0}^{\infty}\frac{\rho_\lambda^{i+1}}{\lambda+2}\eta^{i+1} - k\Gamma^{i+1}\sum_{\lambda=0}^{\infty}\frac{u_\lambda^{i+1}}{\lambda+2}\eta^{i+1} - \sum_{\lambda=0}^{\infty}\frac{h_\lambda^i}{\lambda+1}\eta^\lambda. \tag{41}$$

This completes the derivation of u^{i+1}, v^{i+1}, T^{i+1}, ρ^{i+1}, and Γ^{i+1} at iteration step $i+1$ from known values u^i, v^i, T^i, ρ^i, and Γ^i at iteration step i. This prescription is followed until convergence with respect to i is established.

Before starting the iteration procedure, values $u^0(\eta)$, $v^0(\eta)$, $T^0(\eta)$, $\rho^0(\eta)$, and Γ^0 must be specified. In this work, values for $u^0(\eta)$, $v^0(\eta)$, $T^0(\eta)$, $\rho^0(\eta)$, and Γ^0 are chosen to be the solution to Eqs. (18)–(21) corresponding to zero-flow conditions ($M_0(\eta) = 0$) as given by Tijdeman [5], and rewritten in Eqs. (42)–(46)

$$u^0(\eta) = \frac{\mathrm{i}}{\gamma}\Gamma^0 p\left(1 - \frac{\mathrm{J}_0(s/\sqrt{\mathrm{i}}\,\eta)}{\mathrm{J}_0(s/\sqrt{\mathrm{i}})}\right), \tag{42}$$

$$T^0(\eta) = \frac{\gamma - 1}{\gamma} p\left(1 - \frac{\mathrm{J}_0(\sigma s/\sqrt{\mathrm{i}}\,\eta)}{\mathrm{J}_0(\sigma s/\sqrt{\mathrm{i}})}\right), \tag{43}$$

$$\rho^0(\eta) = \frac{p}{\gamma} + \frac{\gamma - 1}{\gamma} p \frac{\mathrm{J}_0(\sigma s/\sqrt{\mathrm{i}}\,\eta)}{\mathrm{J}_0(\sigma s/\sqrt{\mathrm{i}})}, \tag{44}$$

$$v^0(\eta) = -\frac{\mathrm{i}kp}{2\gamma}(1 + (\Gamma^0)^2)\eta - \frac{\mathrm{i}^{3/2}kp}{\sigma s}\frac{\gamma - 1}{\gamma}\frac{\mathrm{J}_1(\sigma s/\sqrt{\mathrm{i}}\,\eta)}{\mathrm{J}_0(\sigma s/\sqrt{\mathrm{i}})} + \frac{\mathrm{i}^{3/2}kp}{\gamma s}(\Gamma^0)^2\frac{\mathrm{J}_1(s/\sqrt{\mathrm{i}}\,\eta)}{\mathrm{J}_0(s/\sqrt{\mathrm{i}})}, \tag{45}$$

$$(\Gamma^0)^2 = -\left[\frac{1 - \frac{2\sqrt{\mathrm{i}}}{\sigma s}\frac{\mathrm{J}_1(\sigma s/\sqrt{\mathrm{i}})}{\mathrm{J}_0(\sigma s/\sqrt{\mathrm{i}})} - \frac{2\sqrt{\mathrm{i}}}{\sigma s}\frac{\mathrm{J}_1(\sigma s/\sqrt{\mathrm{i}})}{\mathrm{J}_0(\sigma s/\sqrt{\mathrm{i}})}}{1 - \frac{2\sqrt{\mathrm{i}}}{s}\frac{\mathrm{J}_1(s/\sqrt{\mathrm{i}})}{\mathrm{J}_0(s/\sqrt{\mathrm{i}})}}\right]. \tag{46}$$

Note that the expression for $v(\eta)$ given in Eq. (B13) of Ref. [5] misses a factor of -1 as compared to the correct Eq. (B3) of Ref. [5]. This error proceeds to the final expression for $v(\eta)$ (Eq. (B20) of Ref. [5]). However, expressions for $u(\eta)$, $T(\eta)$, $\rho(\eta)$, and Γ, also given in Ref. [5], are correct. The correct expression for $v(\eta)$ at zero flow [$v^0(\eta)$] is given in Eq. (45) above.

Finally, it should be mentioned that two solutions for Γ^0 exist by taking the square-root of Eq. (46). The two solutions (differing by a minus factor) correspond to running waves along the $+z$ direction and $-z$ direction, respectively. In the next section, numerical results based on the iteration procedure described in the present section, will be discussed for both types of running waves in the case of a non-vanishing gas flow ($M_0(\eta) \neq 0$).

4. Numerical results and discussions

In this section, it will be assumed that the gas flow velocity $w(r)$ can be represented as a linear combination of a flat profile (which represents well fully developed turbulent flow in a cylinder in the absence of temperature gradients being the condition in the absence of acoustic excitation in the present work [17]) and a parabolic profile (corresponding to laminar flow in the absence of temperature gradients)

$$w(r) = \delta\bar{w} + (1 - \delta)2\bar{w}\left(1 - \frac{r^2}{R^2}\right), \tag{47}$$

where $\bar{w}$ is the mean flow through the cylinder (averaged over the cylinder cross-section), and δ measures the degree of turbulence and varies between 0 (laminar flow) and 1 (fully developed turbulent flow). In Table 1, parameters used in the calculations are listed.

Data from calculations on phase speeds (defined as the absolute value of $1/\Gamma''$) and absolute attenuation per unit distance $|\Gamma'|$ are given in Figs. 1(a)–(d) for the case of a flat flow profile (i.e., $\delta = 1$) and a mean flow Mach number equal to 0.1. Two sets of data are depicted in Figs. 1(a)–(d)

Table 1
Material parameters and characteristic dimensions

Parameter	Value	Unit
R_0 (gas constant)	287	J/kg/K
ρ_0 (steady state gas mass density)	0.35	kg/m^3
T_0 (steady state gas temperature)	1000	K
γ (ratio of heat capacities)	1.4	
σ (square-root of Prandtl number)	$\sqrt{0.7}$	
μ (shear viscosity coefficient)	4.15×10^{-5}	N s/m^2
R (cylinder radius)	0.5×10^{-3}	m

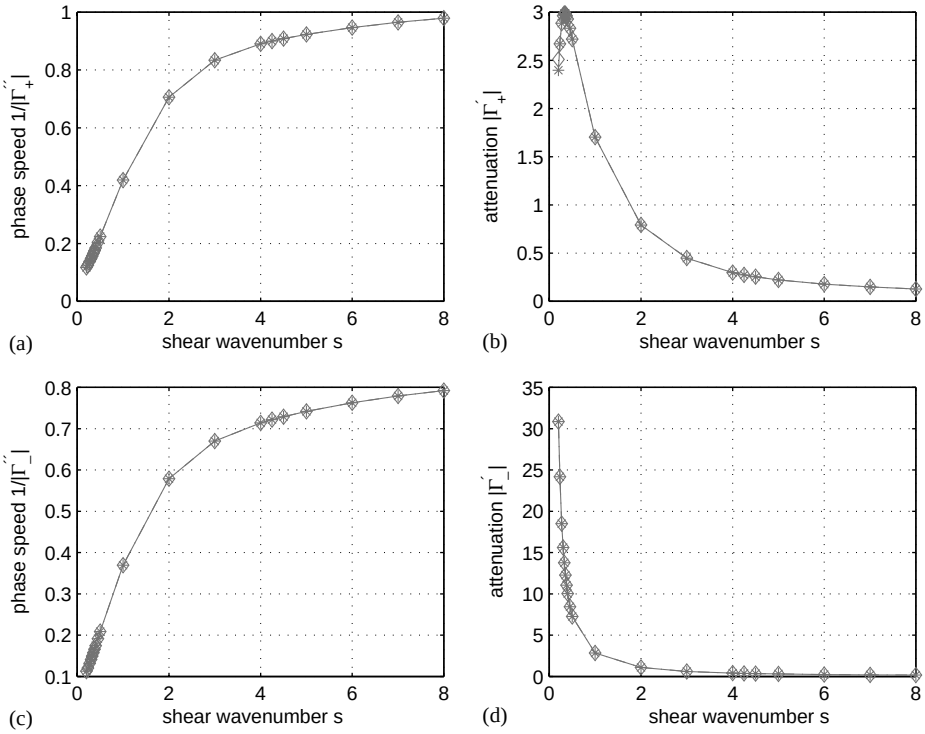

Fig. 1. Calculated results for phase speed $1/|\Gamma''|$ and attenuation $|\Gamma'|$ as a function of shear wavenumber s for the case where the flow profile is flat and the mean flow Mach number equals 0.1. (a)–(d) show results for $1/|\Gamma''_+|$, $|\Gamma'_+|$, $1/|\Gamma''_-|$, and $|\Gamma'_-|$, respectively. The asterisk–solid curve and diamond–dashdotted curve are data obtained using the present model (Frobenius power series expansion method) and analytical results according to Eq. (48), respectively.

corresponding to results obtained by use of the Frobenius infinite power series method as described in the present work ("asterisk–solid curve") and analytical results ("diamond–dashdotted curve"). The agreement is perfect. For the sake of completeness, the analytical expression for Γ, which must be solved iteratively, is given below [11]

$$1-\frac{\Gamma^2}{(1-\mathrm{i}\bar{w}\Gamma)^2}\frac{1}{\gamma}\frac{\mathrm{J}_2\left(\frac{s\sqrt{1-\mathrm{i}\bar{w}\Gamma}}{\sqrt{\mathrm{i}}}\right)}{\mathrm{J}_0\left(\frac{s\sqrt{1-\mathrm{i}\bar{w}\Gamma}}{\sqrt{\mathrm{i}}}\right)}+\frac{\gamma-1}{\gamma}\frac{\mathrm{J}_2\left(\frac{\sigma s\sqrt{1-\mathrm{i}\bar{w}\Gamma}}{\sqrt{\mathrm{i}}}\right)}{\mathrm{J}_0\left(\frac{\sigma s\sqrt{1-\mathrm{i}\bar{w}\Gamma}}{\sqrt{\mathrm{i}}}\right)}=0. \tag{48}$$

Figs. 1(a) and (b) show wave propagation results in the case where acoustic waves propagate along the direction of flow (a subscript "+" on Γ' and Γ'' is introduced here for wave propagation along the direction of flow). Notice, that the phase speed approaches the flow value of 0.1 Mach at low shear wavenumbers as expected. The agreement between data obtained by use of Eq. (48) and data calculated by using the Frobenius power series expansion method is perfect. In particular, Eq. (48) implies that the phase speed approaches $1/(1-\bar{M})$ $(1/(1+\bar{M}))$ to first order in $\bar{M}$ for acoustic wave propagation along (against) the direction of flow as the shear wavenumber approaches infinity $(s\to\infty)$. This result can be easily verified by using the fact that

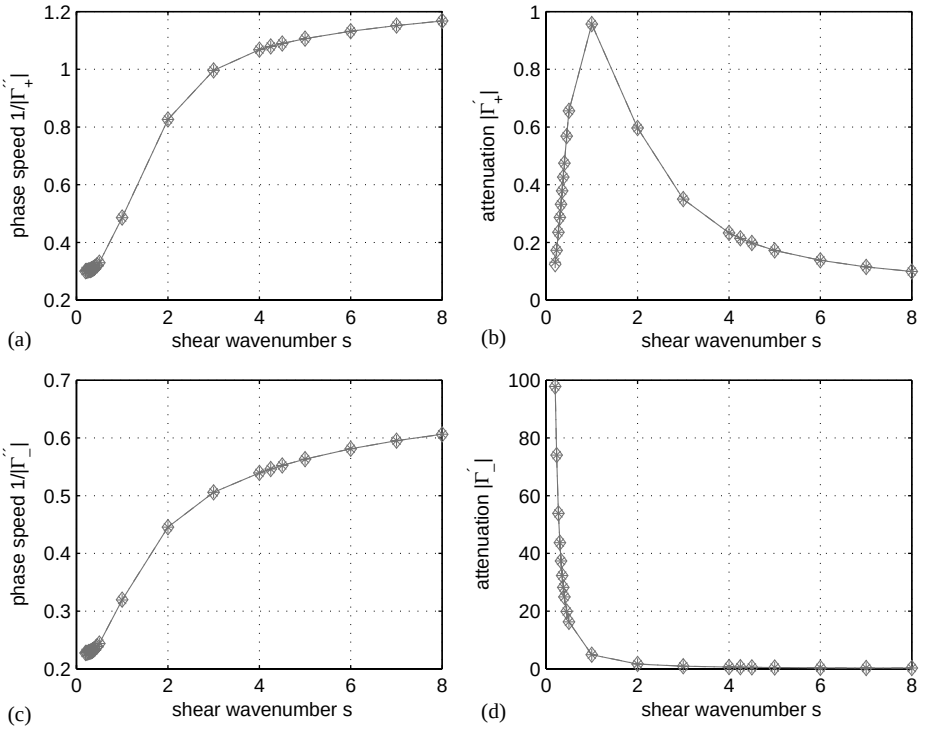

Fig. 2. Calculated results for phase speed $1/|\Gamma''|$ and attenuation $|\Gamma'|$ as a function of shear wavenumber s for the case where the flow profile is flat and the mean flow Mach number equals 0.3. Curve symbols and line codings are as in Fig. 1.

$J_2(x)/J_0(x) \to -1$ as $x \to \infty$ in Eq. (48) and solving for Γ. Values for $1/|\Gamma''_{\pm}|$ have been calculated for $s = 10,\ 15$, and 100 in the case where $\bar{M} = 0.1$ by using Eq. (48) and the present Frobenius power series expansion method. The agreement between the two methods is again perfect and the following values are obtained: $1/|\Gamma''_{+}|$ equals 1.001, 1.032, and 1.089 if s equals 10, 15, and 100, respectively. Similarly, $1/|\Gamma''_{-}|$ equals 0.811, 0.839, 0.890 if s equals 10, 15, and 100, respectively.

Figs. 1(c) and (d) show wave propagation results for the case where acoustic waves propagate against the direction of flow (a subscript "$-$" on Γ' and Γ'' is introduced here for wave propagation against the direction of flow). Apparently, at high shear wavenumbers, attenuation is weak. This is expected since the influence of viscosity becomes less pronounced with increasing shear wavenumbers (refer to Eq. (22)).

In Figs. 2(a)–(d), calculational data are provided for the case of a constant flow profile through the tube and a mean flow equal to 0.3 Mach, i.e., $\bar{w} = 0.3$ Mach. Curve symbols and line codings are as in Figs. 1(a)–(d). Good agreement between analytical results (Eq. (48)) and the present iterative Frobenius power series expansion method is evident. Again, it is found that the phase speed for wave propagation along the direction of flow approaches 0.3 Mach at low shear wavenumbers and attenuation decreases with increasing shear wavenumber. Observe, that attenuation at constant shear wavenumber for wave propagation along the flow $|\Gamma'_{+}|$ decreases

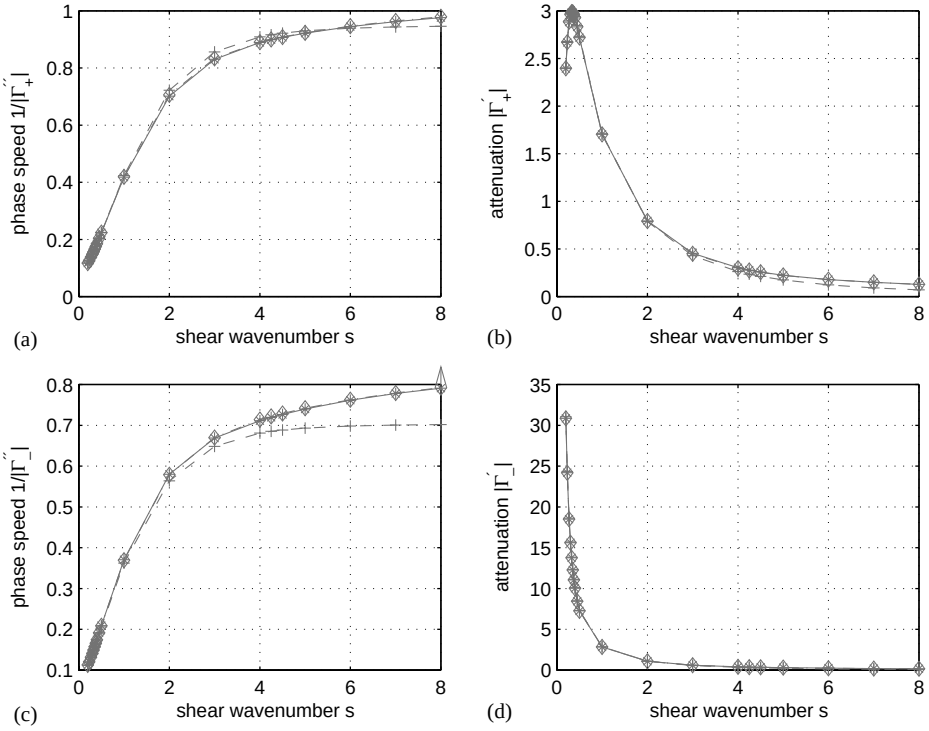

Fig. 3. Calculated results for phase speed $1/|\Gamma''|$ and attenuation $|\Gamma'|$ as a function of shear wavenumber s for the case where the flow profile is parabolic and the mean flow Mach number equals 0.1. (a)–(d) show results for $1/|\Gamma''_{+}|$, $|\Gamma'_{+}|$, $1/|\Gamma''_{-}|$, and $|\Gamma'_{-}|$, respectively. The asterisk–solid curve, diamond–dashdotted curve, and plus–dashed curve are data obtained using the present model (Frobenius power series expansion method), analytical results according to Eqs. (48) and (49) in Ref. [9], respectively.

with flow while $|\Gamma'_-|$ increases with flow at constant shear wavenumber. The same conclusion was found in the paper by Dokumaci [11].

Next, consider the case where the mean flow Mach number equals 0.1 and the flow profile is parabolic ($\delta = 0$). In Figs. 3(a)–(d), three curves are shown. Data using the Frobenius series expansion method (present work) is given by the asterisk–solid curve while the flat flow profile case is given by the diamond–dashdotted curve (the latter curve is identical to the diamond–dashdotted curve in Figs. 3(a)–(d)). Also shown in Figs. 3(a)–(d) is data obtained by solving the cubic polynomial equation (Eq. (49) in Ref. [9]) due to Peat using a variational principle [9] (plus–dashed curve). It is evident that the three models agree quite well in terms of phase speed and attenuation data for wave propagation along the direction of flow. A slight discrepancy is observed between the model of Peat [9] on one side and the present exact model based on the power series expansion method as well as the constant flow profile results. This is to be expected as the assumption that axial acoustic velocities are well represented by a parabolic function in η do not perfectly hold at the higher shear wavenumbers (this limitation was already pointed out by Peat in Ref. [9]). The very good agreement between the approximative model of Dokumaci (flat flow profile [11]) and the present work suggests the use of Dokumaci's approximative solution [11] as a starting guess for the iterative procedure instead of the values at zero-flow conditions (present work). The discrepancy between results based on Peat's model and the present work is mostly

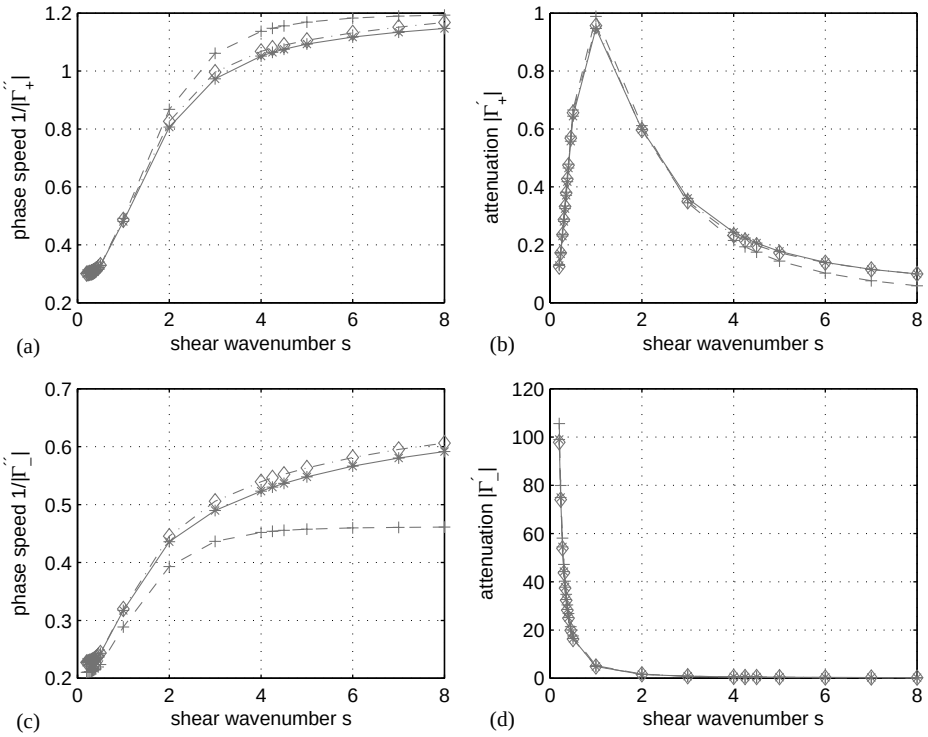

Fig. 4. Calculated results for phase speed $1/|\Gamma''|$ and attenuation $|\Gamma'|$ as a function of shear wavenumber s for the case where the flow profile is parabolic and the mean flow Mach number equals 0.3. (a)–(d) show results for $1/|\Gamma''_+|$, $|\Gamma'_+|$, $1/|\Gamma''_-|$, and $|\Gamma'_-|$, respectively. Curve symbols and line codings are as in Fig. 3.

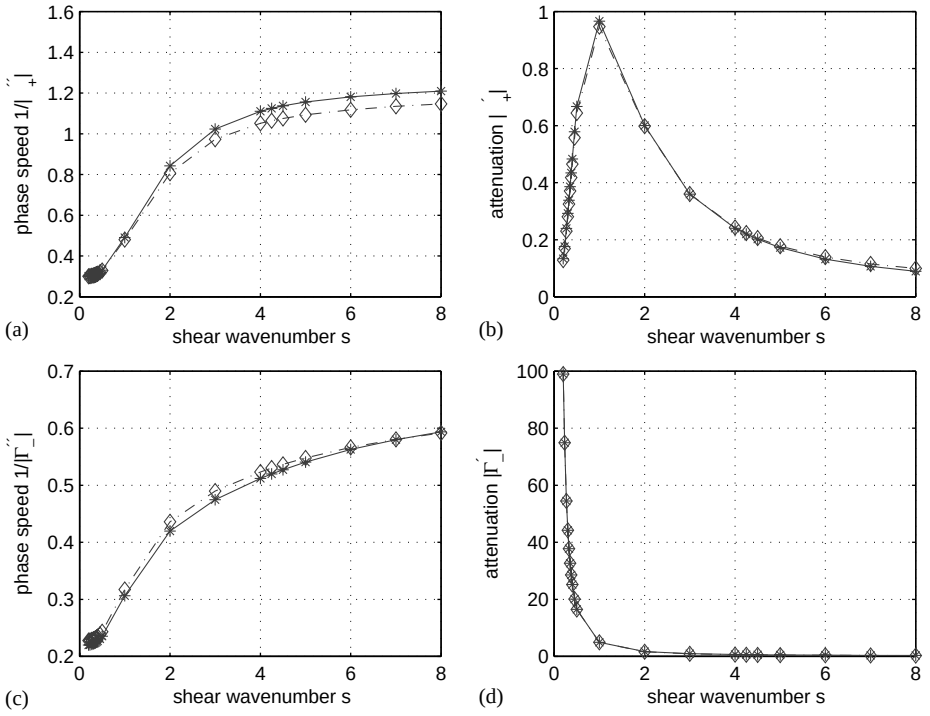

Fig. 5. Calculated results for phase speed $1/|\Gamma''|$ and attenuation $|\Gamma'|$ as a function of shear wavenumber s for the case where the flow profile is parabolic and the mean flow Mach number equals 0.3. (a)–(d) show results for $1/|\Gamma''_+|$, $|\Gamma'_+|$, $1/|\Gamma''_-|$, and $|\Gamma'_-|$, respectively. The asterisk–solid curve and diamond–dashdotted curve are calculated using the exact Frobenius series expansion method and the Frobenius series expansion method where in the latter case all radial velocity terms are set to zero: $v(\eta) = 0$. Also shown is the plus–dashed curve calculated by using of Eq. (49) in Ref. [9].

pronounced in the case of wave propagation against the flow direction at high shear wavenumbers. It should be pointed out that Peat and Kirby recently carried out a "purely" numerical analysis including effects due to radial velocity terms as well as a background temperature gradient [13].

In Figs. 4(a)–(d), data are given for the parabolic flow profile case and a mean flow equal to 0.3 Mach. Same line codings as in Figs. 3(a)–(d) are used. It is evident that results based on a the cubic polynomial equation for Γ [9] deviate somewhat at higher shear wavenumbers while phase speed and attenuation data based on the assumption of a constant flow profile deviate only slightly from those corresponding to the exact Frobenius method (present work).

Next in Figs. 5(a)–(d), results based on the exact Frobenius method (asterisk–solid curve) are compared to those using a similar Frobenius series expansion method except that radial velocity terms are set to zero in the latter case, i.e., $v(\eta) = 0$ (diamond–dashdotted curve). For reference, data using the model in Ref. [9] is plotted again in Figs. 5(a)–(d) (plus–dashed curve). It was postulated by Peat and used by Peat [9] and Astley and Cummings [10] that due to a much smaller cylinder radius in comparison with the acoustic wavelength, one could rationally neglect radial velocity terms altogether. Figs. 5(a)–(d) reveal that this is indeed a reasonable postulate. In the

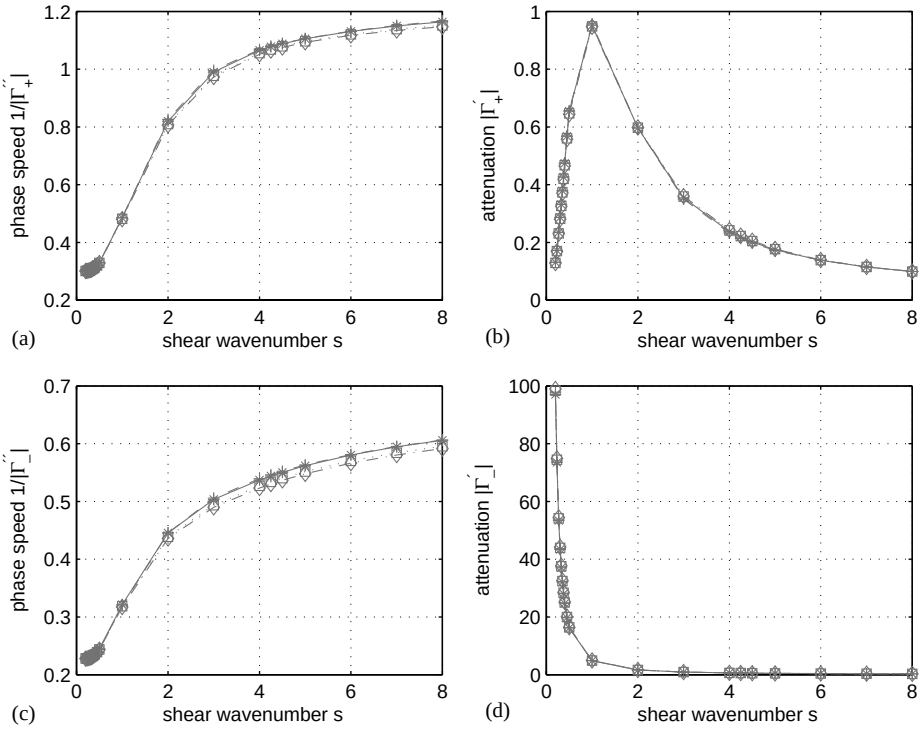

Fig. 6. Calculated results for phase speed $1/|\Gamma''|$ and attenuation $|\Gamma'|$ as a function of shear wavenumber s for the case where the mean flow Mach number equals 0.3. (a)–(d) show results for $1/|\Gamma''_+|$, $|\Gamma'_+|$, $1/|\Gamma''_-|$, and $|\Gamma'_-|$, respectively. The four curves plus–dashed, square–dotted, asterisk–solid, and diamond–dashdotted correspond to $\delta = 1,\ 0.9,\ 0.5$, and 0, respectively.

paper by Astley and Cummings [10], a finite-element model was proposed so as to describe sound propagation in flowing gases confined by cylindrical/rectangular walls. In this work [10], higher order modes were included in the analysis but the assumption that radial velocity terms can be neglected was still be made. The present work clarifies, however, that deviations induced by making this postulate (read: setting radial velocity terms to zero) are greater than deviations caused by approximating the parabolic flow profile by a constant flow profile.

In Figs. 6(a)–(d), data are shown for various flow profiles (δ values) at a constant mean flow equal to 0.3 Mach. The four curves plus–dashed, square–dotted, asterisk–solid, and diamond–dashdotted correspond to $\delta = 1,\ 0.9,\ 0.5$, and 0, respectively. It is evident (as expected from the data already presented in Figs. 1–5) that only small variations in phase speed data as well as attenuation data result from varying the profile parameter δ between 0 and 1.

5. Conclusions

An iterative analytical model based on the dynamic equations governing acoustics in flowing (ideal) gases confined by cylindrical walls is described using the exact Frobenius series expansion

method for the (rather) general case where the flow velocity can be represented by an infinite power series expansion in the radial co-ordinate. It is found that approximating a parabolic flow profile by a constant (flat) profile is a good approximation at low as well as at higher shear wavenumbers (calculations were done up to $s \leqslant 8$). Specifically, in the case where the gas flow velocity $w(r)$ is assumed to be a linear combination of a flat flow profile and a parabolic flow profile, it is also concluded that the error in neglecting radial velocity terms in the analysis is larger than the error due to approximating the flow profile $w(r)$ by its mean value.

References

[1] H.V. Helmholtz, Verhandlungen der Naturhistorisch-Medizinischen Vereins zu Heidelberg Band III, 1863, 16.
[2] G. Kirchhoff, Ueber den Einfluss der Wärmeleitung in einem Gase auf die Schallbewegung, Poggendorfer Annalen 134 (1868) 177–193.
[3] Lord Rayleigh, Theory of Sound II, 2nd Edition, The Macmillan Company, London, 1896, pp. 319–326.
[4] C. Zwikker, C. Kosten, Sound Absorbing Materials, Elsevier, Amsterdam, 1949.
[5] H. Tijdeman, On the propagation of sound waves in cylindrical tubes, Journal of Sound and Vibration 39 (1975) 1–33.
[6] W. Eversman, R.J. Astley, Acoustic transmission in non-uniform ducts with mean flow. Part I: the method of weighted residuals, Journal of Sound and Vibration 74 (1981) 89–101.
[7] R.J. Astley, W. Eversman, Acoustic transmission in non-uniform ducts with mean flow. Part II: the finite element method, Journal of Sound and Vibration 74 (1981) 103–121.
[8] K.S. Peat, The transfer matrix of a uniform duct with a linear temperature gradient, Journal of Sound and Vibration 123 (1988) 43–53.
[9] K.S. Peat, A first approximation to the effects of mean flow on sound propagation through cylindrical waveguides, Journal of Sound and Vibration 175 (1994) 475–489.
[10] R.J. Astley, A. Cummings, Wave propagation in catalytic converters: formulation of the problem and finite element solution scheme, Journal of Sound and Vibration 188 (1995) 635–657.
[11] E. Dokumaci, Sound transmission in narrow pipes with superimposed uniform mean flow and acoustic modelling of automobile catalytic converters, Journal of Sound and Vibration 182 (1995) 799–808.
[12] E. Dokumaci, On transmission of sound in circular and rectangular narrow pipes with superimposed mean flow, Journal of Sound and Vibration 210 (1998) 375–389.
[13] K.S. Peat, R. Kirby, Acoustic wave propagation along a narrow cylindrical duct in the presence of an axial mean flow and temperature gradient, Journal of the Acoustical Society of America 107 (2000) 1859–1865.
[14] B. Karthik, M. Kumar, R.I. Sujith, Exact solutions to one-dimensional acoustic fields with temperature gradients and mean flow, Journal of the Acoustical Society of America 108 (2000) 38–43.
[15] G. Arfken, Mathematical Methods for Physicists, 3rd Edition, Academic Press, Orlando, 1985, pp. 113–115.
[16] M. Willatzen, Sound propagation in a moving fluid confined by cylindrical walls—exact series solutions for radially dependent flow profiles, ACTA Acustica 87 (2001) 552–559.
[17] J. Nikuradse, Gesetzmaessigkeiten der turbulenten Stroemung in glatten Rohren, Forschung auf dem Gebiete des Ingenieurwesens B III (1932) 356.